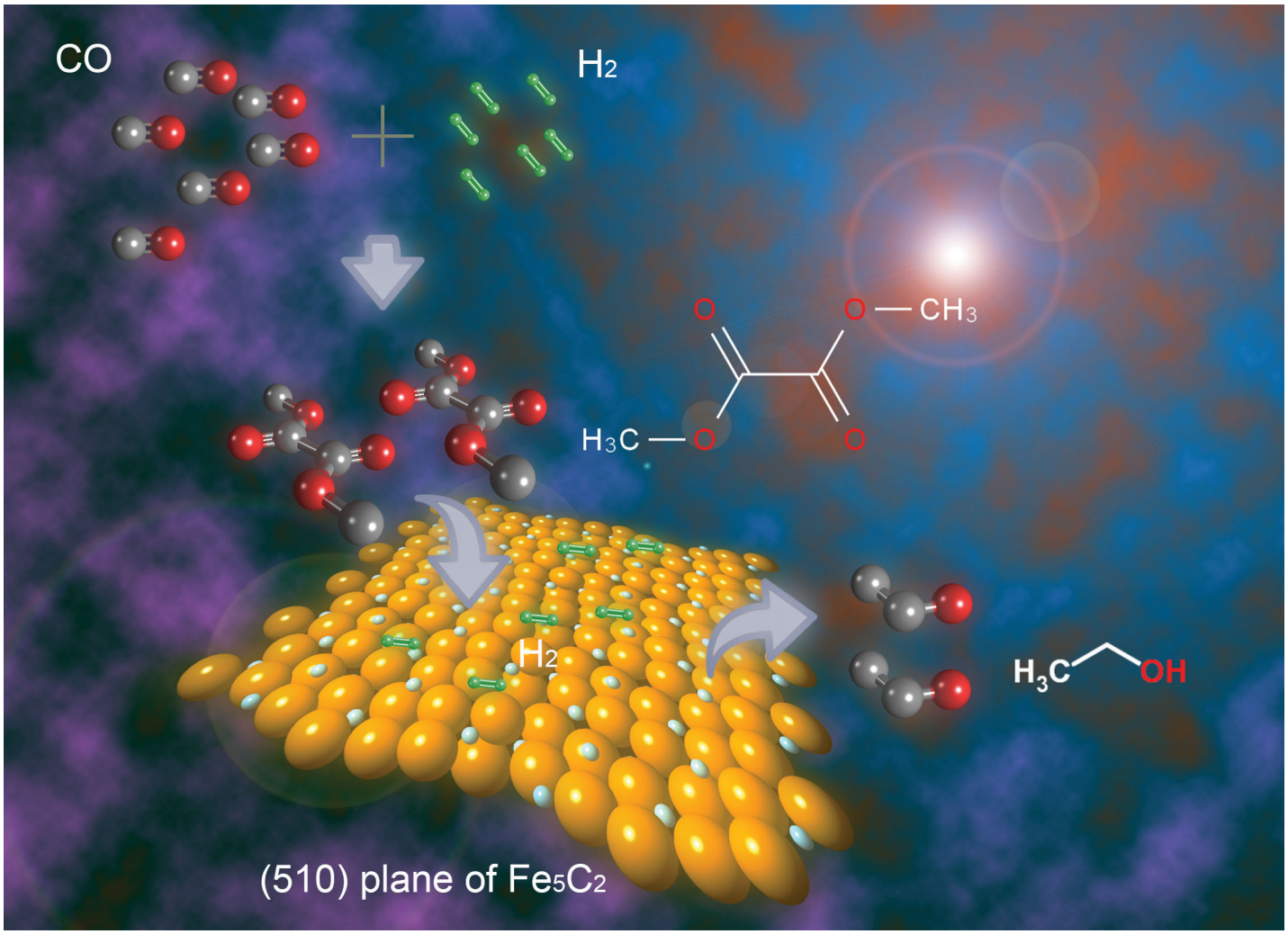

Showcasing the research from Dr Yujun Zhao at Tianjin University and his collaborators at Dalian Institute of Chemical Physics, Pacific Northwest National Laboratory and State University of New York

A Fe_5C_2 nanocatalyst for the preferential synthesis of ethanol *via* dimethyl oxalate hydrogenation

A high efficient Fe_5C_2 catalyst was developed for the preferential synthesis of ethanol *via* dimethyl oxalate hydrogenation. The high stability and low cost of Fe_5C_2 catalyst allow an alternative route for the syngas-to-ethanol technology.

As featured in:

See Yujun Zhao *et al.*, *Chem. Commun.*, 2017, **53**, 5376.

ROYAL SOCIETY OF CHEMISTRY

rsc.li/chemcomm

Registered charity number: 207890

ChemComm

COMMUNICATION

View Article Online
View Journal | View Issue

Cite this: *Chem. Commun.*, 2017, 53, 5376

Received 2nd March 2017,
Accepted 10th April 2017

DOI: 10.1039/c7cc01644a

rsc.li/chemcomm

A Fe_5C_2 nanocatalyst for the preferential synthesis of ethanol *via* dimethyl oxalate hydrogenation†

Jia He,[a] Yujun Zhao,*[ab] Yue Wang,[a] Junhu Wang,[c] Jian Zheng,[b] Hanlei Zhang,[d] Guangwen Zhou,[d] Chongmin Wang,[e] Shengping Wang[a] and Xinbin Ma[a]

A Fe-based catalyst exhibits extremely high selectivity (89.6%) besides excellent catalytic activity in gas-phase dimethyl oxalate hydrogenation. The ethanol formation occurs *via* hydrogenation of methyl acetate instead of ethylene glycol over the active species Fe_5C_2.

Methyl glycolate (MG), one of the intermediate products of dimethyl oxalate (DMO) hydrogenation, comprises both C=O and C–O bonds with different chemical properties, resulting in difficulties in selective hydrogenation. Recent studies have shown that Cu-based catalysts have excellent activity in the hydrogenation of the C=O bonds of the intermediate MG to ethylene glycol (EG), which can be subsequently hydrogenated to ethanol (EtOH) at higher temperature.[1] However, copper catalyst presented insufficient selectivity to ethanol due to the formation of C3–4OH (including butanol, isobutanol, propanol and isopropanol) by the Guerbet reaction.[3] Furthermore, these catalysts had to be used at higher temperatures (543–553 K) to facilitate the formation of EtOH, leading to the accelerated agglomeration of copper species. Therefore, the poor stability of copper is also one of the great challenges for this ethanol synthesis route.[2,3] Recently, metal carbides have been attractive because of their remarkable catalytic behaviours in many hydrogenation reactions.[1–4] Liu *et al.*[5] reported that silica-supported molybdenum carbide (Mo_2C/SiO_2) showed high activity in the hydrogenation of DMO to EtOH. However, the Mo_2C/SiO_2 catalyst was also highly active in the C–C cleavage of DMO simultaneously, resulting in the generation of undesired methanol with a selectivity of 19.4%.[5] Therefore, inhibiting the C–C cleavage of DMO is the key challenge for the industrial application of the Mo_2C-based catalyst in the selective hydrogenation of DMO to ethanol. Due to similarity in the application of Mo carbides and Fe carbides, especially the low cost of Fe carbides, the latter might be a suitable catalyst for the preferential synthesis of EtOH *via* DMO hydrogenation.

Generally, the catalysts (*e.g.* Cu, Ag, and Au) for the hydrogenation of DMO were supported on some porous oxide materials such as SiO_2, Al_2O_3 and ZnO.[1,6,7] In this work, we synthesized bulk Fe carbide catalysts by precipitation followed by carbonization in a methanol–H_2 mixture, which is a novel and facile route for the synthesis of FeC_x NPs compared to the conventional harsh synthesis approach.[8–10] Significant improvements in the activity and selectivity to EtOH are achieved at lower reaction temperature. Moreover, the formation of the Fe_5C_2 species and its role in the hydrogenation of DMO to ethanol were revealed as well.

To identify the formation mechanism of Fe carbides, the phase transition of the iron species in various steps of the preparation procedure was detected by the X-ray diffraction technique (XRD). As shown in Fig. 1A, the diffraction peaks of the sample calcined in air at 673 K are attributed to the a-Fe_2O_3

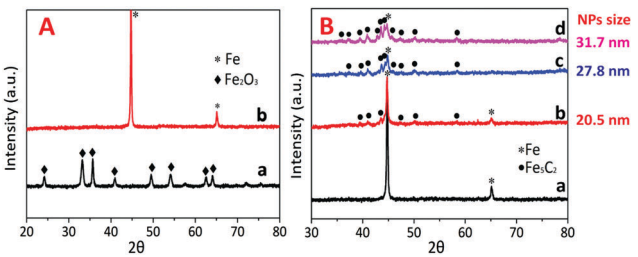

Fig. 1 (A) XRD patterns of catalyst precursors: (a) as-calcined catalyst precursor; (b) as-reduced catalyst precursor. (B) XRD patterns of as-carbonized catalysts: (a) 493K–Fe; (b) 513K–Fe; (c) 533K–Fe; (d) 553K–Fe.

[a] *Key Laboratory for Green Chemical Technology of Ministry of Education, Collaborative Innovation Center of Chemical Science and Engineering, School of Chemical Engineering and Technology, Tianjin University, Tianjin 300072, China. E-mail: yujunzhao@tju.edu.cn; Fax: +86-022-87401818; Tel: +86-022-87401818*

[b] *Institute for Integrated Catalysis, Pacific Northwest National Laboratory, Richland, WA 99352, USA*

[c] *Mössbauer Effect Data Center, Dalian Institute of Chemical Physics, Chinese Academy of Sciences, Dalian, 116023, China*

[d] *Materials Science and Engineering Program & Mechanical Department, State University of New York, Binghamton, New York 13902, USA*

[e] *Environmental Molecular Sciences Laboratory, Pacific Northwest National Laboratory, Richland, WA 99352, USA*

† Electronic supplementary information (ESI) available: Experimental details and characterization data. See DOI: 10.1039/c7cc01644a

phase. Subsequently, upon reduction by H_2 at 653 K, the sample shows only characteristic peaks of metallic Fe at 45° and 66°, indicating the transition of the a-Fe_2O_3 phase to metallic α-Fe (line b in Fig. 1A). The reduced samples are further carbonized in an environment of gaseous methanol and hydrogen at various temperatures (the carbonized samples were denoted as *x*K–Fe, where *x* stands for the carbonization temperature, which is 493, 513, 533 or 553). The diffraction peaks of these samples in the range of 30–70° can be obviously detected (Fig. 1B, a–d), which can be ascribed to the characteristic of the Fe_5C_2 species. The XRD pattern of 533K–Fe (Fig. S2, ESI†) was found to be well consistent with the Fe_5C_2 structure (JCPDS no. 36-1248). Therefore, it implies that Fe_5C_2 can be easily generated by carbonization of α-Fe NPs in methanol–H_2 flow.

Moreover, the carbonization temperature shows an apparent influence on the formation of Fe carbides. As shown in Fig. 1B, with increasing carbonization temperature, the intensity of the diffraction peaks of metallic Fe at 2θ = 45° and 66° is greatly reduced. Meanwhile, the characteristic peaks for Fe_5C_2 are significantly enhanced, indicating that a higher carbonization temperature favors the formation of Fe_5C_2. Moreover, the peak intensity of the 553K-Fe catalyst is similar to that of 533K-Fe. It demonstrates that carbonization treatment at about 533 K is enough for the conversion of metallic Fe into the Fe_5C_2 phase.

Meanwhile, the mean particle sizes of iron carbide NPs follow the order 533K–Fe > 513K–Fe > and 493K–Fe, which were calculated using the Scherrer equation based on the FWHM of the diffraction peak of Fe_5C_2 at 2θ = 40.8°. This finding indicates that the aggregation of Fe_5C_2 particles may occur as the carbonization temperature increases from 493 to 553 K. In addition, it implies that the samples could not be completely carbonized by the methanol–H_2 mixture under the given conditions, since the characteristic peaks for metallic Fe were observed in the carbonized samples. These results coincide well with that obtained from the following MES characterization.

The microstructures and size of the Fe-based catalyst are characterized by TEM analysis. Fig. 2A clearly shows the isolated ellipsoid NPs of Fe species before reduction and carbonization. The size of these particles ranges from 40 to 50 nm. After reduction at 653 K and carbonization in a methanol–H_2 mixture at 533 K, changes in morphology and particle agglomeration are observed in the TEM image (Fig. 2B). As shown in Fig. 2D, the lattice spacing between the neighbouring fringes is 0.205 nm, which should be ascribed to the (510) plane in monoclinic Fe_5C_2.[11] These issues are also evidenced by the above XRD results. Furthermore, it can also be observed that the surface of the Fe_5C_2 NPs is slightly covered with amorphous carbon. Therefore, the Fe_5C_2 NPs should be encapsulated by a shell of amorphous carbon after carbonization treatment, which was also reported by Yang *et al.*[12]

Mössbauer spectroscopy (MES) is a powerful tool to ascertain the accurate structure of iron phases, and the distribution of iron-based materials. Prior to MES characterization, the catalyst samples (*x*K–Fe, *x* = 513, 533 and 553) were obtained by carbonization in methanol–H_2 flow at three different temperatures: 513 K, 533 K and 553 K, respectively. The MES results are

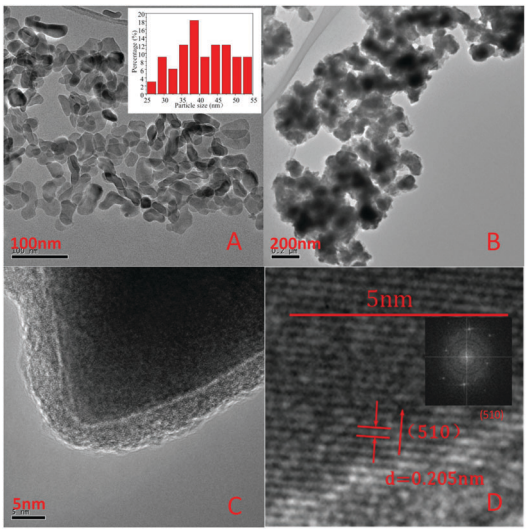

Fig. 2 TEM images of 533K–Fe: (A) as-calcined catalyst precursor; (B) as-carbonized catalyst; (C and D) HRTEM images of the as-carbonized catalyst.

Table 1 Mössbauer parameters of the carbonized catalysts[e]

Sample	IS[a] (mm s^{-1})	QS[b] (mm s^{-1})	H_{hf}[c] (T)	Area[d] (%)	Assignment
513K–Fe	0.25	0.09	21.71	22.26	Fe_5C_2(I)
	0.20	−0.01	18.85	16.78	Fe_5C_2(II)
	0.12	−0.05	10.42	14.20	Fe_5C_2(III)
	0.00	0.01	33.43	35.34	Fe
	1.19	1.82	—	11.42	Fe^{2+}
533K–Fe	0.25	0.08	21.61	28.62	Fe_5C_2(I)
	0.21	0.02	19.11	26.79	Fe_5C_2(II)
	0.12	−0.05	10.42	30.27	Fe_5C_2(III)
	0.00	0.01	33.27	7.55	Fe
	1.19	1.81	—	6.77	Fe^{2+}
553K–Fe	0.22	0.08	21.66	38.86	Fe_5C_2(I)
	0.20	0.01	19.13	35.63	Fe_5C_2(II)
	0.12	−0.05	10.42	21.11	Fe_5C_2(III)
	0.00	0.04	32.91	4.54	Fe
	1.19	1.81	—	1.85	Fe^{2+}

[a] Isomer shift (relative to Fe). [b] Quadrupole splitting. [c] Hyperfine magnetic field. [d] Relative spectral area. [e] All the catalyst samples were carbonized at a total pressure of 2.5 MPa for 24 hours in an environment of gaseous methanol and hydrogen.

shown in Fig. S1, ESI† and Table 1. Metallic iron is identified based on the sextet with a hyperfine magnetic field (H_{hf}) of 32.9–33.4 T.[13] The sextets with a H_{hf} of 10.4–21.7 T could be attributed to Fe_5C_2.[14–16] There is a super paramagnetic (spm) doublet with an isomer shift (IS) of 1.91 mm s^{-1} and a quadrupole splitting (QS) of 1.81 mm s^{-1} attributable to the Fe^{2+} species. It indicates that the content of Fe_5C_2 species significantly increased from 53.24% in the 513K–Fe catalyst to 85.68% in the 533K-Fe catalyst. Upon further increasing the carbonization temperature, the total amount of Fe_5C_2 species in 553K-Fe catalysts (93.7%) is slightly higher than that in 533K-Fe catalysts (85.69%). These results agree well with the changes in Fe_5C_2 species revealed by XRD characterization.

The Fe-based catalysts were applied in the synthesis of ethanol *via* vapor-phase DMO hydrogenation and the results

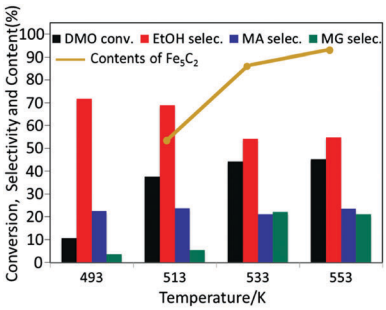

Fig. 3 Effect of carbonization temperature on the catalytic performance of *x*K–Fe. Reaction conditions: T = 473 K, $P(H_2)$ = 2.5 MPa, H_2/DMO = 180, WHSV = 0.2 h^{-1}.

are shown in Fig. 3. In order to elucidate the activity contributing to DMO hydrogenation, both low temperature and high temperature hydrogenation have been performed. The catalytic performance of *x*K-Fe catalysts was first examined at a reaction temperature of 473 K, which was much lower than the carbonization temperature so that further carbonization could be avoided during the reaction. The catalyst sample 493K-Fe yields the lowest activity in the hydrogenation of DMO, among the as-prepared Fe-based catalysts. With the increase of the carbonization temperature, the conversion of DMO increased significantly. But DMO conversion can be hardly increased when the carbonization temperature is higher than 533 K. According to the results of characterization, the increasing carbonization temperature leads to the increase of Fe_5C_2 species in *x*K–Fe catalysts. Therefore, it can be deduced that Fe_5C_2 species might be the key active sites for the hydrogenation activity of Fe-based catalysts. Apparently, in the case of 533K–Fe and 553K–Fe catalysts, the conversion of DMO and selectivity of MG, MA and EtOH are almost the same, which appears to be well explained by the results of MES and XRD characterization mentioned above. Although the contents of Fe_5C_2 species in 553K-Fe catalysts (93.7%) are a little higher than the 533K-Fe catalysts (85.68%), they could probably provide identical amounts of Fe_5C_2 active sites because the measured $D_{Fe_5C_2}$ of 553K-Fe catalysts (30.7 nm) is larger than that of 533K-Fe catalysts (26.1 nm). So, the 533K-Fe and 553K-Fe catalysts present comparable catalytic performances. It was also suggested that 533 K is the optimum temperature for the carbonization of Fe-based catalysts. Interestingly, the 493K-Fe catalyst shows the highest selectivity to EtOH and the lowest selectivity to MG although its apparent activity is the lowest among the four catalysts. The big difference in reaction rates among the tandem reactions might be the reason. Due to the lower conversion of DMO on the 493K-Fe catalyst, we can assume that this catalyst could not supply enough active sites for the activation of DMO since Fe_5C_2 species are the lowest in this catalyst, thus leading to the lower DMO hydrogenation rate. The extremely low MG selectivity might be because of the higher activity of this catalyst in the further hydrogenation of MG. Meanwhile, no EG was formed on the catalysts and MA selectivity was significantly high, suggesting that MG was preferentially hydrogenated through the activation of C–O instead of the C=O bond. The selectivity to EtOH shows an apparent decrease with the carbonization temperature of the catalysts, which can be ascribed to the insufficient active sites for the further activation of MG or MA. Estimating the intrinsic reaction rate of these reactions will help in understanding the changes in the product distribution on various catalysts. But this issue is just beyond the scope of this topic.

The vapor-phase DMO hydrogenation over the Fe-based catalyst results in a remarkable difference in the reaction route, compared to that achieved over the traditional Cu-based catalyst. As previously reported in the hydrogenation of DMO over the Cu-based catalyst at 473 K, MG was firstly synthesized, which could be subsequently hydrogenated to EG with a selectivity as high as 96% by the adsorption of its C=O bonds. But there was hardly any MA formed in this process. When the reaction temperature was increased from 473 to 553 K, ethanol (selectivity ~ 83%) was formed *via* further hydrogenation of EG. But some byproducts such as 2-butanol, butanol and propanol (total selectivity ~ 10–20%) were also generated through the Guerbet reaction on the basic sites of Cu/SiO_2.[1] Fig. 4A presents the performance of the 533K-Fe catalyst for DMO hydrogenation as a function of reaction temperature (473–553 K). As the temperature increases, the selectivity to ethanol was significantly improved accompanied by the decrease in the selectivities to MA and MG. It is noteworthy that EG can be nearly ignored in the reaction products in the case of this Fe-based catalyst. The formation of a larger amount of MA suggests that C–O bonds of MG can be easily activated than C=O bonds by Fe_5C_2 catalysts. Therefore, the generation of EtOH *via* DMO hydrogenation over this carbonized Fe-based catalyst could be likely *via* further hydrogenation of intermediate MA instead of EG (as shown in Scheme 1). A similar reaction route for the hydrogenation of DMO to EtOH has also been proposed by Liu *et al.* over the Mo_2C/SiO_2 catalyst.[5] This reaction route is different from that over the copper-based catalyst which favours the activation of C=O on Cu^+ sites; thus, intermediate MG is mainly hydrogenated to EG instead of MA.[1–3] In the synthesis of ethanol *via* DMO hydrogenation, the Fe-based catalyst not only shows superior DMO conversion (100%) and remarkably high EtOH selectivity (89.8%), but also a lower reaction temperature compared with the copper-based catalysts.

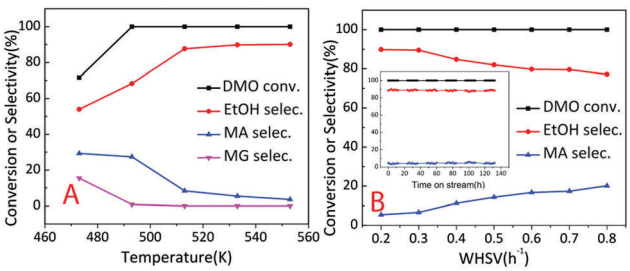

Fig. 4 DMO hydrogenation over the 533K-Fe catalyst as a function of (A) reaction temperature (2.5 MPa, WHSV = 0.2 h^{-1}, H_2/DMO = 180 (mol mol^{-1})). (B) WHSV (2.5 MPa, 533 K, H_2/DMO = 180 (mol mol^{-1})). Inset: Stability of the 533K-Fe catalyst (2.5 MPa, 533 K, H_2/DMO = 180 (mol mol^{-1}), WHSV = 0.2 h^{-1}).

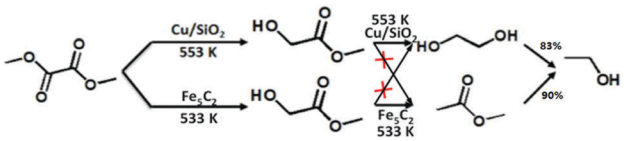

Scheme 1 The reaction pathway of hydrogenation of DMO on Fe_5C_2 and Cu/SiO_2.

For the convenience of a comparison with the Mo_2C/SiO_2 catalyst, the reaction was conducted by varying the WHSV of DMO. As shown in Fig. 4B, with the increase of WHSV from 0.2 to 0.8 h^{-1}, the conversion remained constant at 100% and the selectivity to ethanol gradually decreased from 90% to 80% for the Fe-based catalyst. However for Mo_2C/SiO_2, when the WHSV increases up to 0.5 h^{-1}, the selectivity to ethanol dramatically declined to less than 10%.[5] Additionally, we did not find the additional formation of methanol on the Fe-based catalyst, which presents an obvious advantage in preventing DMO from dissociation *via* the C–C bond compared to the Mo_2C/SiO_2 catalyst. Moreover, the Fe carbide catalyst exhibits excellent stability in the hydrogenation of DMO to ethanol (inset in Fig. 4B). Therefore, the Fe carbide catalyst might be a suitable catalyst for the preferential synthesis of ethanol from DMO, due to its superior catalytic performance from an industrial viewpoint.

In conclusion, Fe-based catalysts carbonized by the methanol–H_2 method exhibit noteworthy improvements in both hydrogenation activity and EtOH selectivity. The formation of a larger amount of MA and a trace of EG suggests that C–O bonds of MG can be easily activated than C=O bonds by this Fe-based catalyst. Therefore, ethanol can be preferentially synthesized from DMO *via* the hydrogenation of intermediate MA instead of EG on the Fe carbide catalyst. It was also found that higher carbonization temperature favours the formation of Fe_5C_2 species, which are considered as the important active sites for the reaction. The Fe-based catalyst carbonized at 533 K exhibited superior catalytic performance and stability with a significantly high ethanol selectivity of 89.6%. This work might provide a meaningful inspiration on catalyst design to achieve high activity, selectivity and stability in the preferential synthesis of ethanol *via* DMO hydrogenation.

We are grateful for the financial support from the National Natural Science Foundation of China (21276186, 21325626, 91434127, U1510203), and the Tianjin Natural Science Foundation (13JCZDJC33000). Mössbauer spectroscopy (MES) was performed at the Mössbauer Effect Data Center in the Dalian Institute of Chemical Physics, CAS. Parts of the work was performed at Pacific Northwest National Laboratory (PNNL). PNNL is operated by Battelle for the Department of Energy under Contract DE-AC05-76RLO1830. We would also like to express our special thanks to Johannes Lercher and Donald M Camaioni (PNNL) for their constructive suggestions to this study.

Notes and references

1 J. Gong, H. Yue, Y. Zhao, S. Zhao, J. Lv, S. Wang and X. Ma, *J. Am. Chem. Soc.*, 2012, **134**, 13922–13925.
2 S. Zhao, H. Yu, Y. Zhao, B. Wang, Y. Geng, J. Lv, S. Wang and J. Gong, *J. Catal.*, 2013, **297**, 142–150.
3 Y. Song, J. Zhang, J. Lv, Y. Zhao and X. Ma, *Ind. Eng. Chem. Res.*, 2015, **54**, 9699–9707.
4 Y. Zhu, X. Kong, X. Li, G. Ding, Y. Zhu and Y. Li, *ACS Catal.*, 2014, **4**, 3612–3620.
5 Y. Liu, J. Ding, J. Sun, J. Zhang, J. Bi, K. Liu, F. Kong, H. Xiao, Y. Sun and J. Chen, *Chem. Commun.*, 2016, **52**, 5030–5032.
6 Y. Zhu, X. Kong, S. Zhu, F. Dong, H. Zheng, Y. Zhu and Y. Li, *Appl. Catal., B*, 2015, **166–167**, 551–559.
7 X. Kong, X. Zhang and J. Chen, *Catal. Commun.*, 2015, **65**, 46–50.
8 K. Yang, W. Xu, Y. Zhang, W. Zheng and X. Wang, *Chem. Res. Chin. Univ.*, 2010, **26**, 348–351.
9 X. Dong, Z. Zhang, Q. Xiao, X. Zhao, Y. Chuang, S. Jin, W. Sun, Z. Lin, Z. Zheng and H. Yang, *Chem. Mater.*, 2009, **21**, 5136.
10 J. Sun, Y. Gao and R. Che, *Mater. Lett.*, 2010, **64**, 680–683.
11 S. Hong, D. Chun, J. Yang, H. Jung, H. Lee, S. Hong, S. Jang, J. Lim, C. Kim and J. Park, *Nanoscale*, 2015, **7**, 16616–16620.
12 C. Yang, H. Zhao, Y. Hou and D. Ma, *J. Am. Chem. Soc.*, 2012, **134**, 15814–15821.
13 J. Su, Y. Gao and R. Che, *Mater. Lett.*, 2010, **64**, 680–683.
14 A. Scrimshire, A. L. Lobera, R. Kultyshev, P. Ellis, S. D. Forder and P. A. Bingham, *Croat. Chem. Acta*, 2015, **88**(4), 531–537.
15 J. X. Xie, H. M. Torres Galvis, A. C. J. koeken, A. Kirilin, A. Iulian Dugulan, M. Ruitenbeek and K. P. Jong, *ACS Catal.*, 2016, **6**, 4017–4024.
16 S. Hong, D. Chun, J. Yang, H. Jung, H. Lee, S. Hong, S. Jang, J. Lim, C. Kim and J. Park, *Nanoscale*, 2015, **7**, 16616–16620.